Journal of Ovonic Research Vol. 15, No. 4, July - August 2019, p. 205 - 213

PREPARATION OF Ho-TiO_2 BASED PHOTOANODE FOR IMPROVED ENERGY CONVERSION EFFICIENCY OF DYE SENSITIZED SOLAR CELL

I. AHMAD[a,*], M. H. KHAN[a], M. HAFEEZ[a], M. IQBAL[b]
[a]*Chemistry Department, Azad Jammu & Kashmir University, Muzaffarabad 13100, AJK, Pakistan*
[b]*Physics Department, Azad Jammu & Kashmir University, Muzaffarabad 13100, AJK, Pakistan*

Holmium doped titanium dioxide (Ho-TiO_2) nanoparticles synthesized by sol-gel method were used to fabricate photoanode for dye sensitized solar cell (DSSC). Powder X-ray diffraction (PXRD) technique was used to confirm the single phase crystalline structure of nanoparticles, UV-Vis absorption spectroscopy was used to probe the optical properties whereas scanning electron microscope (SEM) showed the surface morphology and average particle size of the nanoparticles. Photocurrent density-voltage (*J-V*) characteristics measured under simulated solar light (AM 1.5G, 100 mW cm^{-2}) showed that DSSCs based on Ho doped TiO_2 photoanode have fairly higher power conversion efficiency (PCE) in comparison with undoped TiO_2 based DSSC. Namely the DSSC with optimum 1 wt.% Ho doping exhibited a PCE (η) of 4.89% (short-circuit current density (*Jsc*) 13.49 mA cm^{-2}, open-circuir current density (*Voc*) 0.57 V and fill factor (*FF*) 0.54) which is 23.48% higher than undoped TiO_2 based DSSC having PCE of 3.96% (*Jsc* 10.98 mA cm^{-2}, *Voc* 0.59 V and *FF* 0.54) under similar conditions. Enhancement in power conversion efficiency (PCE) was attributed to narrowed bandgap of Ho doped TiO_2 photoanode which expands response in visible region to effectively utilize sunlight and acceleration in charge transport by suppressing charge transport resistance.

(Received March 9, 2019; Accepted July 4, 2019)

Keywords: Ho-TiO_2, Dye sensitized solar cell, Short-circuit current density, Efficiency improvement

1. Introduction

Energy consumption and demand is increasing globally due to increasing world population at an alarming rate. As the development of modern society is based on the availability of uninterrupted supply of energy, therefore, it is need of time to explore renewable sources of energy [1-6]. Solar energy is the most abundant source of energy which can be converted to electrical energy through photovoltaic devices [7, 8]. Among solar devices dye sensitized solar cells (DSSC) have got considerable attention due to easy availability of its materials, economical, lightweight and its high power conversion efficiency in diffused light [9-14]. A DSSC is composed of a semiconductor photoanode sensitized by adsorbed dye molecules, redox electrolyte and a platinum counter electrode [15-18]. In a DSSC photoanode is mainly responsible for the photocurrent density and the efficiency of device as it transports photo-inducded electrons from excited dye molecules adsorbed on its surface [10, 19, 20]. Among photoanode materials anatase TiO_2 is the most investigated material which has given excellent photostability, low toxicity and superior device efficiency [10, 13, 21, 22]. As it absorbs mostly in UV region which is only 5% of solar spectrum due to its wide bandgap (3.2 eV) limits its large scale use. And numerous dyes cannot inject electrons into conduction band (CB) of TiO_2 due to insufficient driving force which can be expressed as the difference between excited state of dye molecules and conduction band (CB) of TiO_2. Therefore, in order to enhance energy harvesting efficiency of DSSC device alternative

* Corresponding author: ikhtiarahmad@gmail.com

photoanodes that should exhibit better photoresponse under irradiation of visible light are urgently needed [23-26].

DSSCs based on nanocrystalline TiO_2 photoanode have got huge attention since its breakthrough study by Gratzel in 1991 [13]. To improve the efficiency of DSSC various modifications have been reported like surface modification of TiO_2 photoanode by $TiCl_4$ (which increases photocurrent by enhancing lifetime of electrons) [27], combining TiO_2 with other semiconductors (SnO_2, ZnO, ZrO_2, Nb_2O_5, In_2O_3, WO_3 and La_2O_3) [15, 28-30], doping metals (Cu, Zn. Cr, Mg, Nb, Ta) [31-36] and nonmetals (N, S, F, I) [37-40]. Doping of TiO_2 with nonmetals reduces bandgap of semiconductor, improves visible light response and enhances DSSC efficiency. For example Guo et el. doped TiO_2 with varying amount of nitrogen and have got maximum 46% improvement in efficiency with 0.4% N doping as compared to undoped TiO_2 based DSSC [41]. Similarly Yang and co-workers applied F doped TiO_2 photoanode to DSSC and obtained 11.3% higher device efficiency [42]. However doping of nonmetals is limited due to their electronegativity and small size [43]. Doping of metals to photoanode enhances photocurrent and reduces the electron recombination in DSSC. Zhou et al. [31] enhanced the visible light properties of TiO_2 by Cu doping and got almost 20 % higher DSSC performance by improving short circuit current density. Tong et al. [44] introduced intermediate bands in the bandgap of TiO_2 through W doping and enhanced DSSC efficiency from 6.64 % to 7.42 %. Neetu et al. [45] narrowed bandgap of TiO_2 photoanode by aluminum doping and got pretty high IPCE and overall efficiency of DSSC. Li et al. [46] decorated Au on urchin like TiO_2 microspheres by one step hydrothermal method. DSSC based on this Au-TiO_2 microspheres have given pretty high efficiency (7.21%) in comparison with only urchin like TiO_2 microspheres (η=6.10%) and pure P25 (η=5.19%) based DSSCs. Some researchers modified TiO_2 photoanode by co-doping with different metals or non-metals and got the benefit of synergic effect of co-doping for enhanced photovoltaic performance. Park et al. [27] synthesized highly visible light responsive Zr/N-TiO_2 nanoparticles by sol-gel method and got excellent DSSC efficiency (12.62%). Tanyi et al. [47] enhanced efficiency of DSSC by co-doping TiO_2 with La and Mg. Liu et al. [48] co-doped TiO_2 with Zn and Mg and got excellent photovoltaic results. Majority of researchers focused on doping TiO_2 with main group and transition metals whereas very few groups introduced f-block elements into TiO_2 photoanode. Doping of TiO_2 with rare-earth elements could be very beneficial because 4f electrons can change optical, photo-physical and chemical properties due to possibility of electronic transitions in 4f orbital [49]. Zhang et al. [50] modified TiO_2 electrode with cerium doping and got excellent photovoltaic response by tuning bandgap positively. Yao et al. [51] had harvested 33.3% higher DSSC efficiency by modifying photoanode with Nd-TiO_2 nanorods. Improvement in efficiency was due to better electron injection properties as well as due to reduced electron transfer resistance. Similarly Wei et al. and Qin et al. enhance visible light response of photoelectrode by introducing Sm into TiO_2 nanocrystals and got excellent DSSC performance [49, 52].

In present work, Ho doped TiO_2 nanoparticles were prepared by modified sol-gel technique and structural, optical and morphological characterizations were carried out by X-ray diffraction, UV-vis absorption spectroscopy and scanning electron microscopy (SEM) respectively. Photoanodes were fabricated from synthesized materials and photovoltaic properties of DSSCs were probed through current-density vs voltage (*J-V*) and incident photon to current conversion efficiency (IPCE) while charge transport across the DSSC was examined by electrochemical impedance spectroscopic (EIS) analysis technique.

2. Experimental

2.1. Synthesis

All the chemicals used in this work were of analytical reagent grade and were used as received without further purification. Ho doped TiO_2 nanoparticles with different Ho content (0.5, 1 and 2 wt.%) were synthesized by sol-gel method. In a typical procedure solution (1) was prepared by slowly adding 0.1mol of titanium isopropoxide into 100 mL anhydrous ethanol at room temperature under vigorous stirring. A second liquid medium (2) was prepared by mixing 30 mL ethanol and 10 mL acetic acid. Appropriate amount of $Ho(NO_3)_3$. $5H_2O$ was dissolved into

solution (2) and further stirred for half an hour. And then solution (1) was dropwise added into solution (2) while constant stirring. 10-15 mL deionized water was added into it and allowed the mixture to stir for four hours at 60 ^{o}C and then left for aging overnight at room temperature. Thick gel formed was dried at 100 ^{o}C for 12 hours and then calcined in furnace at 450 ^{o}C for 4 hours with ramp rate of 5 ^{o}C per minute. For comparison pure TiO_2 nanoparticles were also synthesized under same conditions.

2.2. Preparation of electrodes and DSSC fabrication

The nanocrystalline TiO_2 photo-anode and platinum counter electrodes were fabricated on fluorine doped tin oxide (FTO) glass substrates using doctor blade technique. Glass substrates were first sonicated in detergent solution for 15 minutes and then rinsed with distilled water, acetone and ethanol respectively and finally dried in oven. To prepare printing paste for photoanode, 5g Ho-TiO_2 or un-doped TiO_2 nanoparticles powder was added into 20 mL absolute ethanol, followed by addition of 3 mL acetic acid and 1.5 mL Triton x-100. The resultant mixture was sonicated for 15 min in ultrasonic bath. Then it was vigorously mixed in mortar and pestle until a homogeneous paste formed which was concentrated at 40 ^{o}C to achieve viscous paste. It was printed on cleaned FTO substrates and annealed in furnace at 450 ^{o}C for 30 minutes. When cooled down to room temperature, these printed electrodes were dipped into N719 dye solution (0.3 mM) prepared in a mixture of tert-butanol, DMSO and acetonitrile (1:1:1) in dark for 24 hours. These photoanodes were taken out, rinsed with ethanol and dried at room temperature.

FTO glass substrates for counter electrodes were cleaned using same procedure for photoanode substrates. Platinum paste (Solaronix, Platisol T/SP) was coated on conducting side by doctor blade procedure and electrodes were annealed in furnace at 450 ^{o}C for 10 minutes.

DSSCs were assembled from these dye adsorbed working electrodes and Pt printed counter electrode in a sandwich type fashion with printed sides facing each other. Electrodes were hold together by binding clips, electrolyte (solaronix, iodolyte AN-50) was injected between the electrodes with the help of a syringe and binder clips were loosed alternatively so that electrolyte cover entire active cell area.

2.3. Characterization

Crystalline phase of undoped and Ho doped TiO_2 nanoparticles was measured using PANAnalytical X-ray diffractometer with Cu-Kα radiation. UV-vis absorption studies were performed using spectrophotometer (Shimadzu UV-1601, japan) in the range of 200-800 nm. Surface morphologies of prepared nanoparticles were observed with scanning electron microscopy (SEM) Jeol JSM-6510LV. Photocurrent-voltage (*J-V*) measurements of DSSC devices were done on a Keithley 2400 source meter under illumination by solar simulator (SOL3A, Oreal) at AM 1.5 G illumination with light intensities of 100 mW cm^{-2}. Incident photon to current conversion efficiency (IPCE) properties were studied using QEX10, PV Measurements system. Electrochemical impedance spectroscopic (EIS) studies were carried out under illumination (with xenon lamp of 450 W) at 100 mW cm^{-2} using solar simulator (Oriel SOL3A,) set at bias voltage of Voc. Measurements were obtained from 100 mHz to 200 kHz and Bio-Logic, Z-fit software was used to fit spectras.

3. Results and discussion

Structural characterization of Ho doped TiO_2 and pure TiO_2 nanoparticles were carried out by X-ray diffraction measurements. Figure 1 displays the XRD pattern of undoped TiO_2 and 0.5%, 1% and 2 wt.% Ho doped TiO_2 nanoparticles. XRD results indicate that all the samples have pure anatase structure (matched with standard JCPDS card no 21-1272), having no individual holmium oxide peak, suggesting that Ho ions are precisely doped into TiO_2 lattice. Ho doped samples have relatively lower peak intensities than undoped TiO_2. Crystallite size of nanoparticles was estimated with Scherrer equation [53] from full width at half maximum for major diffraction peak (101) which reveals that Ho doping cause a decrease in particle size. Due to insertion of Ho into TiO_2 lattice diffraction peaks can shift towards lower or higher angle [54], as can be seen in Fig. 1.

In Ho doped samples Peak broadening and shifting towards lower diffraction angle at (101), (004), (200) and (105) have been observed as compared to un-doped TiO_2 which confirms successful doping.

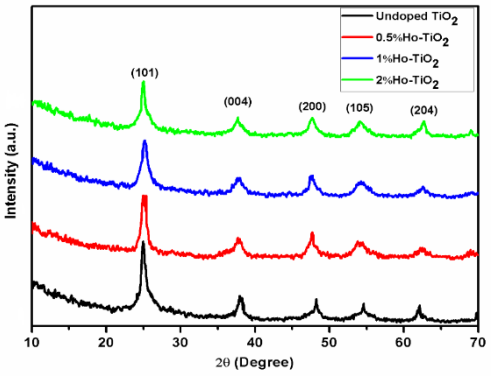

Fig. 1. XRD pattern of synthesized TiO_2 and Ho-TiO_2 nanoparticles.

Surface morphology of the undoped and Ho doped TiO_2 particles was determined with scanning electron microscopy (Figure 2) and particles sizes were estimated with imageJ software. Pure TiO_2 nanoparticles have cubical shape with wide size distribution ranging from 30-70 nm. Cubical shape retained in 0.5 wt.% Ho doped TiO_2 nanoparticles while particle size reduced (nearly 28-55 nm), whereas 1 wt.% Ho doped TiO_2 particles are of elongated and some irregular shapes and is nearly 25-50 nm. In 2 wt.% Ho doped TiO_2 sample, particles with little agglomeration are of different shapes and size is nearly 30-55 nm. SEM images clearly shows that upon Ho doping into TiO_2, particles size decreases thus providing higher specific surface area which is beneficial for sufficient dye loading on photoanode.

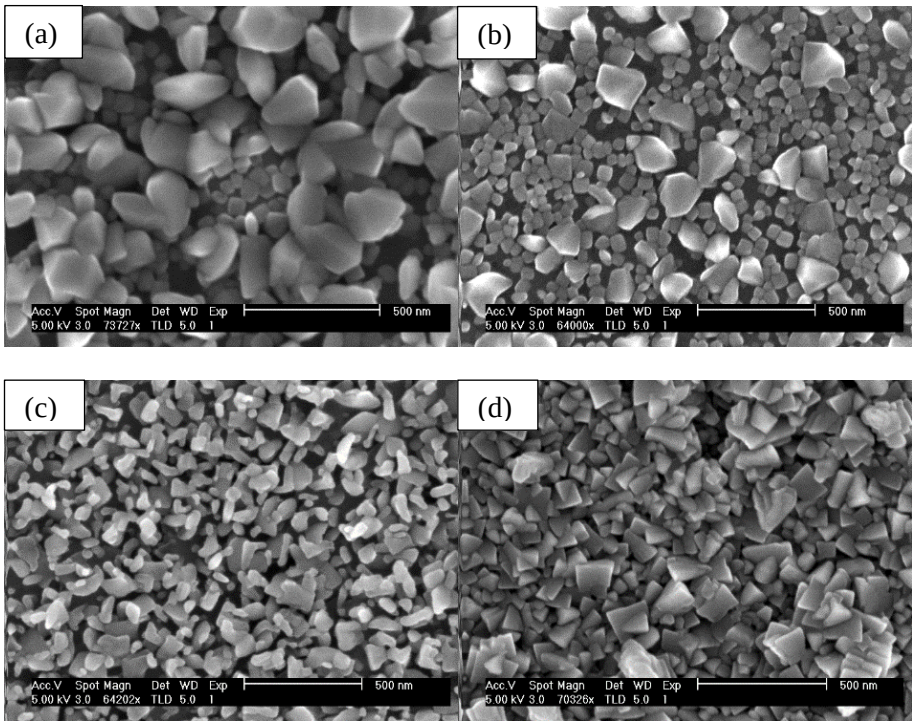

Fig. 2. SEM images of synthesized TiO_2 (a) and Ho-TiO_2 (b-d) nanoparticles.

To study the effect of Ho doping on optical properties of TiO_2 UV-vis absorption studies have been carried out of all synthesized samples. The absorption spectra of undoped TiO_2 and Ho doped TiO_2 nanoparticles are given in figure 3 which indicate that on Ho doping absorption increased and absorption window widened towards longer wavelength which is beneficial for DSSC photoanode material. In undoped TiO_2 sample, absorption occurs due to electronic transitions from O-2p to Ti-3d orbital while in doped samples it is Ho-4f orbital electrons which induced red shift in absorption spectrum [55]. This means Ho doping cause the narrowing of band gap of TiO_2 nanoparticles as calculated by plotting $(\alpha h\nu)^{1/2}$ vs hν photon energy shown in Fig. 3 in inset. Comparing 0.5 wt.%, 1 wt.% and 2 wt.% Ho doped samples it is observed absorption increases from 0.5-1 wt.% and decreases from 1-2 wt.% doping level.

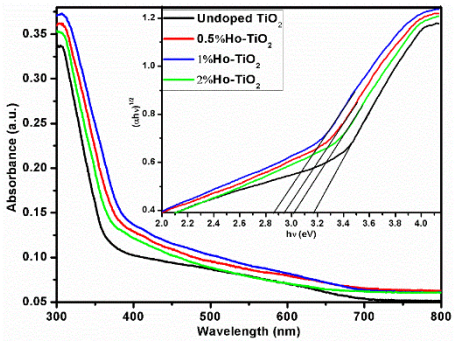

Fig. 3. UV-vis absorption spectra and in inset $(ahv)^{1/2}$ vs hν of TiO_2 and Ho-TiO_2 nanoparticles.

Table 1. Crystallite size and bandgap of synthesized TiO_2 and different Ho-TiO_2 nanoparticles.

Sample	*Crystallite size (nm)	*Bandgap (eV)
Undoped TiO_2	20.60	3.17
0.5 wt.% Ho-TiO_2	15.70	2.95
1 wt.% Ho-TiO_2	13.20	2.86
2 wt.% Ho-TiO_2	16.32	3.02

*Crystallite size was calculated using Scherrer equation from major diffraction peak (101) while bandgap was calculated from UV-vis data by plotting $(\alpha h\nu)^{1/2}$ vs hν photon energy.

Dye adsorption capability of photoanodes were determined by measuring UV-vis absorption spectra of dye adsorbed photoanodes. Fig. 4 shows that Ho doped TiO_2 based photoanodes have higher absorption than undoped TiO_2 based photoanode. Thus it is confirmed that Ho doping into TiO_2 enhances its dye adsorption ability and expands absorption in visible region. Higher dye adsorption facilitate wide range of solar light capturing and thus producing more electrons by photoanode which ultimately lead to better DSSC efficiency.

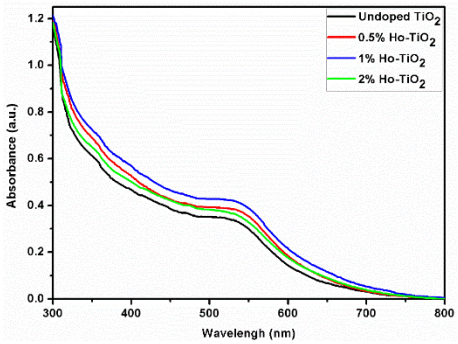

Fig. 4. UV-Vis absorption spectra of dye (N719) sensitized photoanodes.

To explore the effect of Ho doping on photovoltaic properties of TiO_2, DSSCs were fabricated from un-doped TiO_2 and Ho doped TiO_2 nanoparticles. Current density-voltage (J-V) characteristics of DSSCs measured under standard illumination conditions (AM 1.5G, 100 mW/cm^2) are given in Figure 5 while detailed photovoltaic parameters are given in table 2. Results showed that DSSCs based on Ho doped photoanodes (0.5 wt%, 1 wt% and 2 wt%) have higher device efficiency compared to undoped TiO_2 based photoanode. DSSC efficiency increases on increasing Ho content in photoanode up to 1 wt.% doping and then decreases on further increasing holmium quantity. DSSC with 1 wt% Ho-TiO_2 have given maximum energy harvesting efficiency (η) of 4.89% with Jsc of 13.49 mA cm^{-2}, Voc 0.57 V, FF 0.54. This is 23.48% higher efficiency (η) than un-doped TiO_2 based DSSC which have overall efficiency (η) of 3.96%. Photovoltaic parameters indicate that Ho doped DSSCs have higher Jsc and overall efficiency (η) but no significant effect on Voc and fill factor of devices, it means Ho doping increases electron density in TiO_2 and promote electron transport properties by reducing electron transfer resistance. Improvement in efficiency can be ascribed to enhanced absorption which favors more effectively consuming UV-Visible light, increment in Jsc arising from efficient electron injection, reduced charge transport resistance and translates to higher PCE [56, 57]. A downfall in efficiency at 2 wt.% Ho doping was possibly due to formation of defects in crystal lattice which trap the photo-generated electrons, thus lowering the Jsc and hence the whole efficiency of device [31].

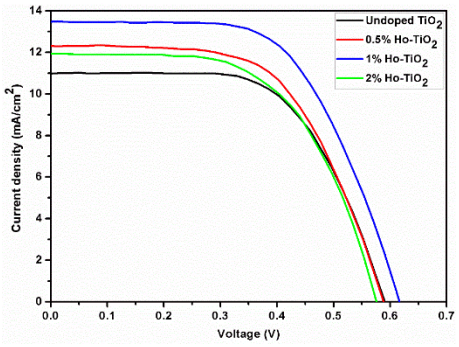

Fig. 5. J-V curves of DSSCs fabricated from TiO_2 and Ho-TiO_2 nanoparticles.

Table 2. Photovoltaic properties of synthesized TiO_2 and different Ho-TiO_2 based DSSCs.

DSSC	Jsc (mA cm^{-2})	Voc (V)	FF	PCE (%)
Undoped TiO_2	10.98	0.59	0.54	3.96
0.5 wt.% Ho-TiO_2	12.30	0.57	0.53	4.21
1 wt.% Ho-TiO_2	13.49	0.57	0.54	4.89
2 wt.% Ho-TiO_2	11.92	0.58	0.53	4.07

Incident photon to current conversion efficiency (IPCE) measurements: IPCE of device is the ratio between total number of electrons produced by light in external circuit and incident photons number. Fig. 6 displays the IPCE spectra of un-doped and Ho doped TiO_2 based DSSCs, measured between 300-900 nm. It shows that Ho doped devices have fairly higher IPCE compared to pure TiO_2 based device in entire region. At 540 nm maximum IPCE values observed for Ho doped TiO_2 (0.5%, 1%, 2%) based DSSC were 52%, 55.40% and 49.5% respectively whereas at this wavelength un-doped TiO_2 based DSSC has 47.62%. The higher IPCE values of Ho doped devices can be attributed to increased dye adsorption, higher absorption in visible region and efficient charge transport properties.

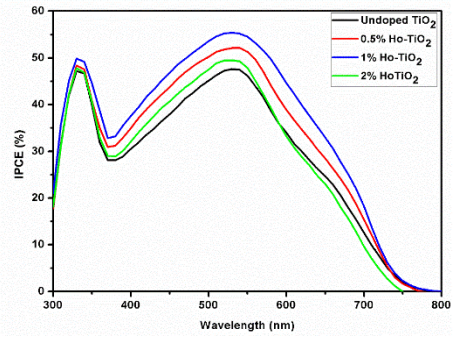

Fig. 6. IPCE profile of synthesized TiO_2 and Ho-TiO_2 based DSSCs.

Electrochemical impedance spectroscopy (EIS) is an important spectroscopic method to study charge transport in DSSCs [44]. To investigate the change in electron transport in DSSC upon doping TiO_2 with Ho electrochemical impedance spectroscopic analysis have been carried out. In EIS Nyquist plot generally two semicircles are found, small semicircle represent electron transport resistance at the interface of FTO/TiO_2 photoanode and electrolyte/Pt counter electrode. Bigger semicircle in low frequency region represents the charge transport across interface of mesoporous photoanode/dye/electrolyte [44, 58, 59].

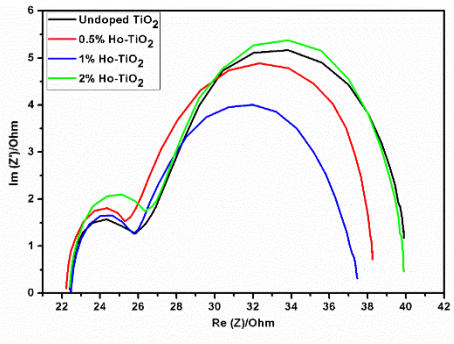

Fig. 7. Nyquist plot of DSSCs measured under standard solar irradiation (AM 1.5G).

EIS spectra of DSSCs based on un-doped TiO_2 and Ho doped TiO_2 are presented in Figure 7. In these spectra it can be seen that larger semicircle is decreasing upon Ho doping into TiO_2 which means acceleration in electron transport is taking place due to decrease in charge transport resistance resulting in increased *Jsc* and efficiency of cells. This effect is more pronounced in DSSCs with 0.5 wt.% and 1 wt.% Ho doping and when doping amount increased to 2 wt.% semicircle size again increases resulting a decrease in *Jsc* and efficiency of cell. Thus EIS studies inferred that DSSC based on 1 wt.% Ho doping in TiO_2 has lowest charge transport resistance, higher Jsc and hence higher efficiency of device.

4. Conclusion

In summary Ho-TiO_2 nanoparticles prepared by sol-gel method were successfully utilized to fabricate photoanode for N719 sensitized DSSCs. X-ray diffractograms confirm the successful incorporation of Ho into TiO_2 anatase lattice as there were no individual holmium oxide peaks. UV-vis absorption measurements showed red shift in absorption thus narrowing the bandgap which is useful for efficient utilization of sunlight. Photovoltaic properties of DSSCs were greatly enhanced by Ho doping into TiO_2. DSSC with 1 wt % Ho-TiO_2 yielded best PCE (η) 4.89% while under similar conditions of one sun illumination AM 1.5 undoped TiO_2 based DSSC have given PCE (η) of 3.96%. IPCE measurements followed the same pattern of J-V measurements, i.e. 1

wt% Ho- TiO_2 exhibited maximum value of 55.40% at λ_{max} 540 nm in comparison with undoped TiO_2 which have resulted a maximum of 47.62%. EIS studies revealed that electron transport increases after Ho doping by suppressing charge transport resistance. Hence Ho doping into TiO_2 made it a better option as a photoanode for DSSC in comparison with pure TiO_2.

Acknowledgments

The authors greatly acknowledge higher education commission (HEC) of Pakistan for grant of PhD fellowship under Indigenous 5000 PhD fellowship scheme (112-24036-2PS1-357) to carry out this project.

References

[1] N. S. Lewis, Science **315**, 798 (2007).
[2] T. R. Cook, D. K. Dogutan, S. Y. Reece, Y. Surendranath, T. S. Teets, D. G. Nocera, Chemical reviews **110**, 6474 (2010).
[3] D. G. Nocera, Inorganic chemistry **48**, 10001(2009).
[4] M. K. Nazeeruddin, S. Zakeeruddin, R. Humphry-Baker, M. Jirousek, P. Liska, N. Vlachopoulos, V. Shklover, C.-H. Fischer, M. Grätzel, Inorganic Chemistry **38**, 6298 (1999).
[5] C. Grätzel, S. M. Zakeeruddin, Materials Today **16**, 11 (2013).
[6] M. K. Nazeeruddin, P. Pechy, T. Renouard, S. M. Zakeeruddin, R. Humphry-Baker, P. Comte, P. Liska, L. Cevey, E. Costa, V. Shklover, Journal of the American Chemical Society **123**, 1613 (2001).
[7] G. Konti, G. C. Vougioukalakis, M. Bidikoudi, A. G. Kontos, C. Methenitis, P. Falaras, Polyhedron **82**, 12 (2014).
[8] M. Grätzel, Nature **414**, 338 (2001).
[9] Y. Duan, N. Fu, Q. Liu, Y. Fang, X. Zhou, J. Zhang, Y. Lin, The Journal of Physical Chemistry C **116**, 8888 (2012).
[10] A. Hagfeldt, G. Boschloo, L. Sun, L. Kloo, H. Pettersson, Chemical reviews **110**, 6595 (2010).
[11] D. Wei, International Journal of Molecular Sciences **11**, 1103 (2010).
[12] B. C. O'Regan, J. R. Durrant, Accounts of Chemical Research **42**, 1799 (2009).
[13] B. O'regan, M. Grfitzeli, nature **353**, 737 (1991).
[14] X. Lü, X. Mou, J. Wu, D. Zhang, L. Zhang, F. Huang, F. Xu, S. Huang, Advanced Functional Materials **20**, 509 (2010).
[15] R. Jose, V. Thavasi, S. Ramakrishna, Journal of the American Ceramic Society **92**, 289 (2009).
[16] C. Dong, W. Xiang, F. Huang, D. Fu, W. Huang, U. Bach, Y.-B. Cheng, X. Li, L. Spiccia, Nanoscale **6**, 3704 (2014)
[17] S. J. Lim, Y. S. Kang, D.-W. Kim, Electrochemistry Communications **12**, 1037 (2010).
[18] F. Sauvage, D. Chen, P. Comte, F. Huang, L.-P. Heiniger, Y.-B. Cheng, R. A. Caruso, M. Graetzel, Acs Nano **4**, 4420 (2010).
[19] S. Ardo, G. J. Meyer, Chemical Society Reviews **38**, 115 (2009).
[20] K. Kalyanasundaram, Dye-sensitized solar cells, EPFL press, 2010.
[21] M. Law, L. E. Greene, J. C. Johnson, R. Saykally, P. Yang, Nature Materials **4**, 455 (2005).
[22] Q. Huang, G. Zhou, L. Fang, L. Hu, Z.-S. Wang, Energy & Environmental Science **4**, 2145 (2011).
[23] Z.-S. Wang, Y. Cui, Y. Dan-oh, C. Kasada, A. Shinpo, K. Hara, The Journal of Physical Chemistry C **112**, 17011 (2008).
[24] J. Liu, Y. Duan, X. Zhou, Y. Lin, Applied Surface Science **277**, 231 (2013).
[25] M. An'amt, S. Radiman, N. Huang, M. A. Yarmo, N. Ariyanto, H. Lim, M. Muhamad, Ceramics International **36**, 2215 (2010).

[26] J.-Y. Park, C.-S. Kim, K. Okuyama, H.-M. Lee, H.-D. Jang, S.-E. Lee, T.-O. Kim, Journal of Power Sources **306**, 764 (2016).
[27] J.-Y. Park, K.-H. Lee, B.-S. Kim, C.-S. Kim, S.-E. Lee, K. Okuyama, H.-D. Jang, T.-O. Kim, RSC Advances **4**, 9946 (2014).
[28] C.-S. Chou, F.-C. Chou, Y.-G. Ding, P. Wu, Solar Energy **86**, 1435 (2012).
[29] J. Qian, P. Liu, Y. Xiao, Y. Jiang, Y. Cao, X. Ai, H. Yang, Advanced Materials **21**, 3663 (2009).
[30] M. Younas, M. Gondal, M. Dastageer, U. Baig, Ceramics International **45**, 936 (2019).
[31] L. Zhou, L. Wei, Y. Yang, X. Xia, P. Wang, J. Yu, T. Luan, Chemical Physics **475**, 1 (2016).
[32] F. Huang, Q. Li, G. J. Thorogood, Y.-B. Cheng R. A. Caruso, Journal of Materials Chemistry **22**, 17128 (2012).
[33] C. Kim, K.-S. Kim, H. Y. Kim, Y. S. Han, Journal of Materials Chemistry **18**, 5809 (2008).
[34] C. Zhang, S. Chen, L. e. Mo, Y. Huang, H. Tian, L. Hu, Z. Huo, S. Dai, F. Kong, X. Pan, The Journal of Physical Chemistry C **115**, 16418 (2011).
[35] H. Su, Y.-T. Huang, Y.-H. Chang, P. Zhai, N. Y. Hau, P. C. H. Cheung, W.-T. Yeh, T.-C. Wei, S.-P. Feng, Electrochimica Acta **182**, 230 (2015).
[36] J. Liu, H. Yang, W. Tan, X. Zhou, Y. Lin, Electrochimica Acta **56**, 396 (2010).
[37] M. Motlak, M. S. Akhtar, N. A. Barakat, A. Hamza, O.-B. Yang, H. Y. Kim, Electrochimica Acta **115**, 493 (2014).
[38] S. Yang, S. Guo, D. Xu, H. Xue, H. Kou, J. Wang, G. Zhu, Journal of Fluorine Chemistry **150**, 78 (2013).
[39] Q. Sun, J. Zhang, P. Wang, J. Zheng, X. Zhang, Y. Cui, J. Feng, Y. Zhu, Journal of Renewable and Sustainable Energy **4**, 023104 (2012).
[40] Q. Hou, Y. Zheng, J.-F. Chen, W. Zhou, J. Deng, X. Tao, Journal of Materials Chemistry **21**, 3877 (2011).
[41] W. Guo, Y. Shen, L. Wu, Y. Gao, T. Ma, The Journal of Physical Chemistry C **115**, 21494 (2011).
[42] S. Yang, H. Xue, H. Wang, H. Kou, J. Wang, G. Zhu, Journal of Physics and Chemistry of Solids **73**, 911 (2012).
[43] R. Zhang, A. A. Elzatahry, S. S. Al-Deyab D. Zhao, Nano Today **7**, 344 (2012).
[44] Z. Tong, T. Peng, W. Sun, W. Liu, S. Guo, X.-Z. Zhao, The Journal of Physical Chemistry C **118**, 16892 (2014).
[45] I. C. Maurya, A. K. Gupta, P. Srivastava, L. Bahadur, Journal of Solid State Electrochemistry **21**, 1229 (2017).
[46] Y. Li, Y. Zhou, Y. Wang, R. Zhou, Q. Ling, H. Niu, W. Zhang, C. Wang, J. Qiu, Z. Guo, Electrochimica Acta **293**, 230 (2019).
[47 A. Tanyi, A. Ra, Electrochim. Acta **178**, 240 (2015).
[48] Q. Liu, Y. Zhou, Y. Duan, M. Wang Y. Lin, Electrochimica Acta **95**, 48 (2013).
[49] L. Wei, Y. Yang, X. Xia, R. Fan, T. Su, Y. Shi, J. Yu, L. Li, Y. Jiang, RSC Advances **5**, 70512 (2015).
[50] J. Zhang, W. Peng, Z. Chen, H. Chen, L. Han, The Journal of Physical Chemistry C **116**, 19182 (2012).
[51] Q. Yao, J. Liu, Q. Peng, X. Wang, Y. Li, Chemistry–An Asian Journal **1**, 737 (2006).
[52] Y. Qin, Z. Hu, B. H. Lim, W. S. Chang, K. K. Chong, P. Zhang, H. Zhang, Journal of Alloys and Compounds **686**, 803 (2016).
[53] H. P. Klug, L. E. Alexander, X-Ray Diffraction Procedures: For Polycrystalline and Amorphous Materials, Wiley-VCH, New York, 992 (1974).
[54] A. Sahai, Y. Kumar, V. Agarwal, S. Olive-Méndez, N. Goswami, Journal of Applied Physics **116**, 164315 (2014).
[55] M. Saif, M. Abdel-Mottaleb, Inorganica Chimica Acta **360**, 2863 (2007).
[56] C. Xu D. Gao, The Journal of Physical Chemistry C **116**, 7236 (2012).
[57] Z. Han, J. Zhang, W. Cao, Materials Letters **84**, 34 (2012).
[58] Y.-Z. Zheng, X. Tao, L.-X. Wang, H. Xu, Q. Hou, W.-L. Zhou J.-F. Chen, Chemistry of Materials **22**, 928 (2009).
[59] J. Yu, Y. Yang, R. Fan, L. Li, X. Li, The Journal of Physical Chemistry C **118**, 8795 (2014).